Thick Prelaminar Tissue Decreases Lamina Cribrosa Visibility

Katie A. Lucy,[1] Bo Wang,[2,3] Joel S. Schuman,[1] Richard A. Bilonick,[2,4] Yun Ling,[2,5] Larry Kagemann,[6] Ian A. Sigal,[2,3] Ireneusz Grulkowski,[7] Jonathan J. Liu,[7] James G. Fujimoto,[7] Hiroshi Ishikawa,[1] and Gadi Wollstein[1]

[1]Langone Medical Center, Department of Ophthalmology, New York University School of Medicine, New York, New York, United States
[2]UPMC Eye Center, Eye and Ear Institute, Ophthalmology and Visual Science Research Center, Department of Ophthalmology, University of Pittsburgh School of Medicine, Pittsburgh, Pennsylvania, United States
[3]Department of Bioengineering, Swanson School of Engineering, University of Pittsburgh, Pittsburgh, Pennsylvania, United States
[4]Department of Biostatistics, Graduate School of Public Health, University of Pittsburgh, Pittsburgh, Pennsylvania, United States
[5]Department of Epidemiology, Graduate School of Public Health, University of Pittsburgh, Pittsburgh, Pennsylvania, United States
[6]Center for Devices and Radiological Health, Food and Drug Administration, Silver Spring, Maryland, United States
[7]Department of Electrical Engineering and Computer Science, Massachusetts Institute of Technology, Cambridge, Massachusetts, United States

PURPOSE. Evaluation of the effect of prelaminar tissue thickness on visualization of the lamina cribrosa (LC) using optical coherence tomography (OCT).

METHODS. The optic nerve head (ONH) region was scanned using OCT. The quality of visible LC microstructure was assessed subjectively using a grading system and objectively by analyzing the signal intensity of each scan's superpixel components. Manual delineations were made separately and in 3-dimensions quantifying prelaminar tissue thickness, analyzable regions of LC microstructure, and regions with a visible anterior LC (ALC) boundary. A linear mixed effect model quantified the association between tissue thickness and LC visualization.

RESULTS. A total of 17 healthy, 27 glaucoma suspect, and 47 glaucomatous eyes were included. Scans with thicker average prelaminar tissue measurements received worse grading scores ($P = 0.007$), and superpixels with low signal intensity were associated significantly with regions beneath thick prelaminar tissue ($P < 0.05$). The average prelaminar tissue thickness in regions of scans where the LC was analyzable (214 μm) was significantly thinner than in regions where the LC was not analyzable (569 μm; $P < 0.001$). Healthy eyes had significantly thicker average prelaminar tissue measurements than glaucoma or glaucoma suspect eyes (both $P < 0.001$), and glaucoma suspect eyes had significantly thicker average prelaminar tissue measurements than glaucoma eyes ($P = 0.008$). Significantly more of the ALC boundary was visible in glaucoma eyes (63% of ONH) than in healthy eyes (41%; $P = 0.005$).

CONCLUSIONS. Thick prelaminar tissue was associated with impaired visualization of the LC. Healthy subjects generally had thicker prelaminar tissue, which potentially could create a selection bias against healthy eyes when comparing LC structures.

Keywords: image analysis, glaucoma, optic nerve head

The lamina cribrosa (LC), within the optic nerve head (ONH), is composed of a dense and complex meshwork of collagenous fibers. Retinal ganglion cell axons pass through its fenestrations as they exit the eye and form the optic nerve. The LC is considered a primary location for glaucomatous damage, as it is theorized that deformations in the beam and pore microstructure of the LC strangulate axons, which may lead to impaired axonal flow and subsequent damage to retinal ganglion cells.[1-5] The prelaminar tissue, which is composed primarily of retinal ganglion cell axons and their supportive glial cells, has been clinically observed to diminish either naturally with advancing age or with disease.

Optical coherence tomography (OCT) is a noninvasive, in vivo imaging technology capable of visualizing and quantifying the structures of the eye at micrometer scale resolution.[6-9]

Optical coherence tomography has been used extensively to image the ONH and LC. However, in a substantial percentage of eyes it is difficult to fully image the LC with conventional spectral-domain (SD)–OCT imaging, likely due to the signal attenuation that occurs when imaging deeper structures. Swept-source (SS)–OCT uses a longer light source wavelength (1050 nm compared to approximately 850 nm in conventional SD-OCT systems), yielding better tissue penetration. Its light source also has a faster axial scan rate (100,000 A-scans/sec) than conventional SD-OCT (25,000–75,000 A-scans/sec), and the use of a single light detector, compared to the linear array used in SD-OCT, reduces signal drop-off.[10] Swept-source OCT has an axial and transverse resolution of 5 and 15 μm, respectively, in tissue. Furthermore, the fast acquisition rate of SS-OCT allows for the use of advanced scanning patterns,
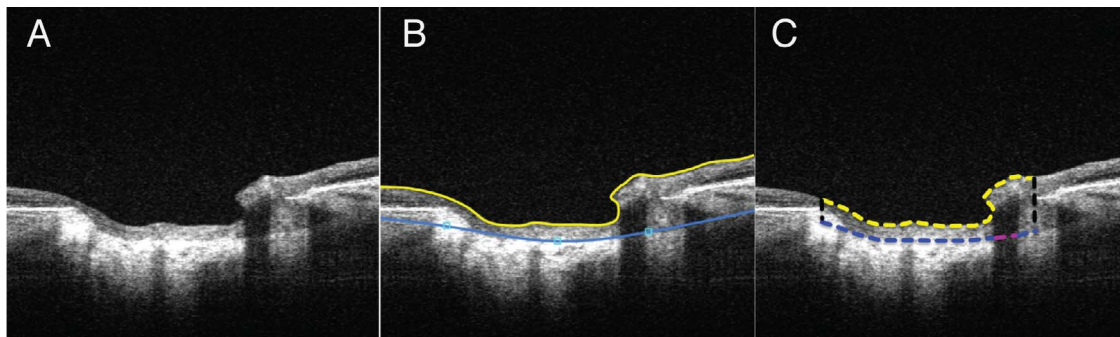
Figure 1. (**A**) Swept source-OCT scan of the ONH of a glaucomatous eye. (**B**) Software view of the delineation of the ILM/anterior prelaminar surface (*yellow line*) and ALC surface (*blue line*). The prelaminar tissue thickness was quantified by (**C**) measuring the average distance between the anterior prelaminar surface (*yellow dashed line*) and the ALC (*blue dashed line*) in the region enclosed by the Bruch's membrane opening (*black dashed lines*). For the measurement of regions in which the ALC was visible, regions such as the area highlighted in *pink* were not included.

which reduces motion artifacts. These advantages make SS-OCT more suitable for capturing images of the LC.[11–15] However, visualization of the LC with SS-OCT remains limited by inherent structural factors, such as media opacities and blood vessel shadowing. We propose that prelaminar tissue also may reduce visualization of the LC. Thick obstructive tissue scatters more light than thinner tissue, attenuating the SS-OCT signal and decreasing LC visualization.

We hypothesized that the LC is better visualized by SS-OCT imaging in regions with thin prelaminar tissue than in regions with thick prelaminar tissue. The purpose of this study was to evaluate the association between prelaminar tissue thickness and visualization of the LC using SS-OCT.

Methods

Subjects

Subjects were sequentially recruited from the Pittsburgh Imaging Technology Trial (PITT) performed at the University of Pittsburgh Medical Center (UPMC) Eye Center. Informed consent was obtained from all subjects, and the institutional review board and ethics committee at the University of Pittsburgh approved this study. This study followed the tenets of the Declaration of Helsinki, and was conducted in compliance with the Health Insurance Portability and Accountability Act.

Subjects were divided into one of three diagnostic categories: healthy, glaucoma suspect, or glaucoma. This distinction was based upon clinical examination and visual field testing (Humphrey field analyzer; Carl Zeiss Meditec, Dublin CA, USA; Swedish interactive thresholding algorithm [SITA] standard, 24-2 test). Healthy subjects were defined as those with a normal clinical examination and visual field glaucoma hemifield tests within normal limits. Glaucomatous eyes were defined as those that showed characteristics of glaucoma during clinical examination (i.e., ONH abnormality: global rim thinning, rim notch, or disc hemorrhage; retinal nerve fiber layer [RNFL] defect) accompanied by typical visual field loss (reproducible glaucoma hemifield tests labeled as outside normal limits on at least two consecutive tests). Glaucoma suspect subjects were defined as those with normal visual field testing but abnormal clinical examination, as defined above. The study included male and female subjects of various ethnicities. Exclusion criteria for the study were nonglaucomatous ocular diseases, nonglaucomatous causes for visual field damage, and intraocular surgery other than noncomplicated cataract or glaucoma surgery.

SS-OCT Image Acquisition

The ONH of all subjects was scanned using a SS-OCT system that has been described previously.[16] A scan volume of 3.5 × 3.5 × 3.6 mm with 400 × 400 × 896 sampling points was used. The scan pattern was orthogonal (consisting of a pair of horizontal and vertical raster scans), and the 400 *x*- and *y*-fast scans were registered to create a 3-dimensional cube of data that eliminated motion artifacts.[17] Both eyes were included from each subject unless the scan from one eye was deemed of insufficient quality due to a lack of proper focus, poor signal, or failure of the motion eliminating registration.

OCT Image Analysis

All manual delineations were completed by an experienced observer that was masked to all clinical information. Analysis in 3-dimensions was achieved by marking every other B-scan or en face component of the 400 × 400 scan volume over the region of the ONH, then reconstructing the 2-dimensional information into a 3-dimensional cube of data. The prelaminar tissue thickness of each eye was considered the axial distance between the vitreous-ONH interface to the anterior laminar surface (Fig. 1). The vitreous-ONH interface was delineated automatically using an in house developed segmentation algorithm. This automatic delineation was assessed and corrected manually whenever it failed to properly distinguish the interface. The prelaminar thickness then was measured in every other frame that contained the ONH (approximately 100 B-scans per eye) by delineating the anterior LC (ALC) boundary and measuring the distance between the ALC and vitreous-ONH interface. The orthogonal view of each B-scan was referenced during delineation in an effort to avoid including border tissue and to represent most accurately the start of the LC area. The Bruch's membrane opening (BMO) and regions of each en face scan in which the LC was visible and analyzable were delineated separately in 3-dimensions using ImageJ (National Institutes of Health [NIH], Bethesda, MD, USA).[18,19] The LC was considered analyzable if the microstructure, composed of individual beams and pores, was visible and clearly distinguishable with sufficient contrast using the en face view of the scan. An experienced observer who regularly assessed LC microstructure quality made the designation of whether the LC microstructure was considered analyzable. The percentage of visible LC microstructure was computed by dividing the area of the maximum projection of the visible LC by the area contained within the BMO.

Regions of each scan in which the ALC boundary was clearly visible were marked in 3-dimensions on every other B-scan that contained the ONH (approximately 100 B-scans per
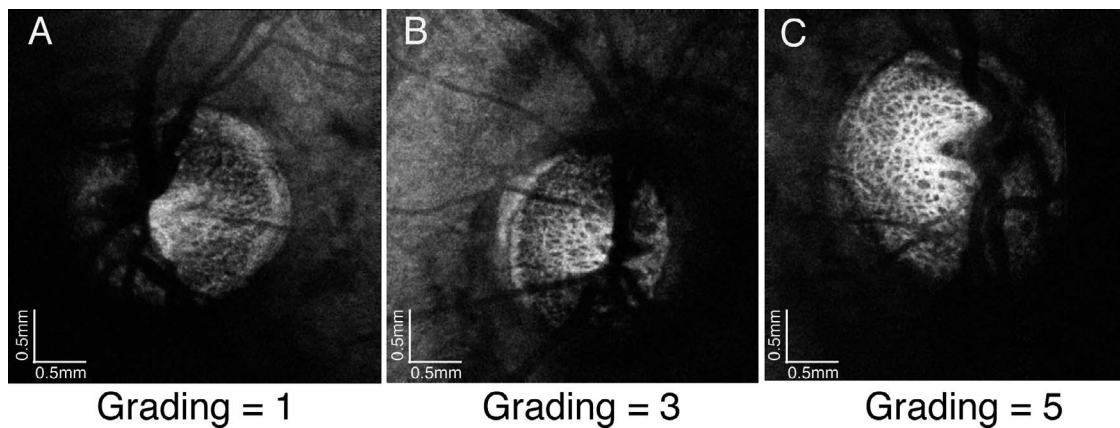
FIGURE 2. Lamina cribrosa subjective grading. **(A)** Poor quality image, **(B)** average quality image, and **(C)** high quality image.

eye) using ImageJ. In the prelaminar tissue calculations, for regions where the ALC was unclear or not visible, the boundary was calculated through interpolation with neighboring regions of visible ALC. The percentage of visible ALC was computed by dividing the area of the visible ALC by the area contained within the BMO.

Reproducibility

To evaluate the intraobserver reproducibility of the manual measurements of prelaminar tissue thickness, the manual measurement procedure was repeated a second time on a randomly selected subset of 19 eyes. The vitreous-ONH interface boundary and the ALC were delineated in a single B-scan from the 19 scans, which as before was used to calculate the average prelaminar thickness of that B-scan. The B-scans were taken randomly from anywhere within the region of the scans defined as the ONH. The imprecision of the measurements, which is the standard deviation of the random error of the measurements, was calculated by separating the measurement error into an estimation of the systematic error of the measurements (bias) and a combination of the true measurement and the random error (which is unknown and cannot be estimated).[20]

LC Quality Assessment

Visualization of the en face LC microstructure (defined as the quality of the scan) was graded subjectively using a scale of 1 to 5, with 1 indicating the worst quality and 5 indicating the best. The a priori grading criteria were based on pore presence, clarity, and contrast as visible on the en face view. Scans graded as a 1 featured little or no visible pores, scans graded as a 3 featured visible pores with unclear definition, and scans graded as a 5 had clear pore boundaries with high beam and pore contrast (Fig. 2). The scoring was done by a single, highly experienced observer in random order without knowledge of subject identification, diagnosis, or any other clinical information. The grader rated the quality of the visible LC; therefore, the score does not reflect the overall scan quality, which was assessed for sufficient quality and a lack of motion artifacts before the scans were selected for the study, as defined in the Methods.

To assess the quality of each scan objectively, the signal intensity of each superpixel (composed of 18 × 18 adjacent pixels) was measured in one en face plane within the LC, per volume. The selected en face image featured the highest quality LC microstructure seen within the scan, and, therefore, subjectively represented the best signal captured in that scan.

A regression line was fitted for each eye to determine the relationship between the LC signal intensity of every superpixel and the prelaminar tissue thickness measured at that superpixel using MATLAB (Mathworks, Natick, MA, USA).[21]

Statistical Analysis

We considered three measures of prelaminar tissue thickness: the average thickness over the entire ONH, the average thickness in regions of scans with analyzable LC microstructure, and the average thickness in regions where the LC was not considered analyzable. The three measures of prelaminar tissue thickness were related to the subjective quality grading and diagnosis using a linear mixed effects model, accounting for the inclusion of both eyes from some subjects. The statistical analysis was performed with R Language and Environment for Statistical Computing software (version 3.2.2).[22]

RESULTS

The subject population consisted of 91 eyes (17 healthy, 27 glaucoma suspect, and 47 glaucoma) from 72 subjects. Subjects with glaucoma were significantly older than healthy subjects, and glaucoma subjects had significantly lower visual field mean deviation (MD) and significantly thinner RNFL measurements than healthy or glaucoma suspects (Table).

The distribution of the LC microstructure visualization quality grading is shown in Figure 3. Most scans were graded at 3 or 4. The average percentage of analyzable LC was 22.7% ± 5.6% for healthy eyes, 21.5% ± 8.7% for glaucoma suspect eyes, and 27.5% ± 7.5% for glaucoma eyes. There was a statistically significantly larger region of LC that could be analyzed in the scans of glaucomatous eyes than in the scans of healthy or glaucoma suspect eyes ($P = 0.033$ and $P = 0.002$, respectively). The average prelaminar tissue thickness was 214

TABLE. Subject Characteristics

Clinical Characteristics	Healthy	Glaucoma Suspect	Glaucoma
Number of eyes	17	27	47
Sex, male/female	15/26	11/15	22/25
Mean age, y	42 ± 15	61 ± 8	65 ± 16
Mean VF MD, dB	−0.70 ± 1.08	0.03 ± 0.80	−6.70 ± 6.18
Mean RNFL, µm	94.23 ± 10.66	89.22 ± 8.85	70.85 ± 10.61

VF, visual field.

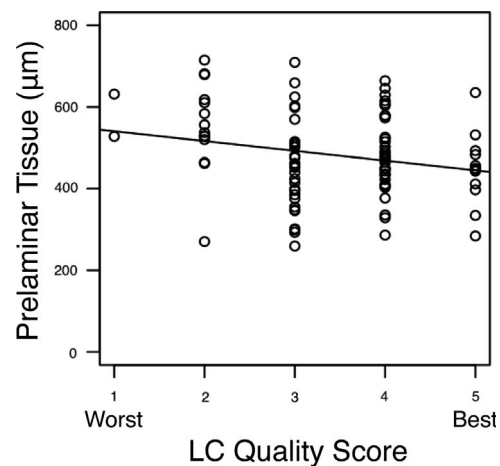**FIGURE 3.** Distribution of LC en face quality grading scores.

FIGURE 4. Distribution of subjective LC quality scores related to the average prelaminar tissue thickness in regions of scans in which the LC was analyzable. Scans with thicker prelaminar tissue were given significantly worse scores ($P = 0.007$).

$\pm$ 96 μm in regions of scans with analyzable LC and 569 $\pm$ 108 μm in regions of scans that did not feature analyzable LC ($P < 0.001$). When the prelaminar tissue thickness in regions of scans that featured analyzable LC was related to the subjective quality grading of the LC, scans with thicker prelaminar tissue had statistically significantly worse LC microstructure visualization scores ($P = 0.007$; Fig. 4).

When the signal intensity of each superpixel of the analyzed en face scan was plotted against the prelaminar tissue thickness measured at that superpixel, high intensity superpixels corresponded with regions of thin prelaminar tissue, and low intensity superpixels corresponded with regions of thick prelaminar tissue. A representative plot that shows the data points from one eye is shown in Figure 5A, with Figure 5B showing the best-fit lines from the plots of all 91 eyes (all slopes significant, $P < 0.05$).

The average total prelaminar tissue thickness was significantly thinner in glaucoma eyes than in healthy or glaucoma suspect eyes (both $P < 0.001$; Fig. 6A). Limiting the analysis to regions of scans in which the LC could be analyzed, there was a substantial reduction in the prelaminar thickness for all clinical diagnostic groups (Fig. 6B). Within this limited analysis examining only regions with analyzable LC, there was a significant difference among all three diagnostic categories, with glaucoma eyes having thinner prelaminar tissue than glaucoma suspect and healthy eyes ($P = 0.008$ and $P < 0.001$, respectively), and glaucoma suspect eyes having thinner prelaminar tissue than healthy eyes ($P < 0.001$). The scale adjusted imprecision of the observer was 2.49 (confidence interval [CI], 1.77–3.70), reflecting excellent measurement reproducibility.

The average percentage of visible ALC was 40.6% $\pm$ 18% for healthy eyes, 57.4% $\pm$ 18% for glaucoma suspect eyes, and 62.9% $\pm$ 17% for glaucoma eyes. A statistically significantly larger region of ALC was observed in glaucomatous eyes than in healthy eyes (Fig. 7; $P = 0.005$). Of these percentages, 38.6% $\pm$ 17% of healthy scans, 56.0% $\pm$ 16% of glaucoma suspect scans, and 60.9% $\pm$ 17% of glaucoma scans corresponded to regions where the LC microstructure was visible using the en face view. Age was not significant in predicting prelaminar tissue thickness or ALC visibility in our linear mixed effects model.

DISCUSSION

Optical coherence tomography imaging is used commonly for in vivo examination of the LC and to determine its involvement

in the glaucomatous process. In this study, we demonstrated that despite the use of SS-OCT with its improved speed and tissue penetration, thick prelaminar tissue was associated with poor LC visualization, and good quality LC visualization was limited to regions with thinner prelaminar tissue. This limitation of current OCT technology should be considered when quantifying LC structures in the population.

We examined a cohort representative of the subjects used in glaucoma studies, composed of healthy, glaucoma suspect, and glaucoma subjects with a wide range of disease severity. Subjective examination of the LC image quality showed the expected bell-shaped distribution of quality scores, with the majority of the images labeled as moderate to good quality (Fig. 3).

The prelaminar thicknesses we recorded were similar to those reported previously.[23–25] Prelaminar thickness was significantly related to LC image quality as determined subjectively by LC visualization grading (Fig. 4) and objectively by the signal intensity in each en face superpixel (Fig. 5). It is likely that thicker prelaminar tissue causes more light scattering and absorption, resulting in blurred visualization of the microstructures of the LC.

Prelaminar tissue was significantly thinner in regions where the LC was analyzable compared to regions where it was not considered analyzable. Overall, the range of average total ONH prelaminar tissue thickness measurements was 250 to 750 μm (Fig. 6A). Little or no LC microstructure visualization was possible in regions of scans where the prelaminar tissue was measured at more than approximately 400 μm (Fig. 6B). Furthermore, we and previous studies reported thicker prelaminar tissue in healthy and glaucoma suspect eyes than glaucomatous eyes.[23,24] There was significantly more visible LC microstructure and ALC in glaucoma eyes than in healthy eyes (Fig. 7). The regions in which the ALC boundary was visible in the B-scan view largely corresponded to regions in which the LC microstructure was visible and analyzable on the en face view. Therefore, thick prelaminar tissue has an important influence on the visualization of the LC in the en face and B-scan views.

As the average prelaminar thickness over the total ONH area was approximately 600 μm in healthy eyes and 400 μm in glaucomatous eyes (Fig. 6A), therefore it is possible that previous studies favored scans with good quality LC microstructure visualization, originating from eyes with advanced
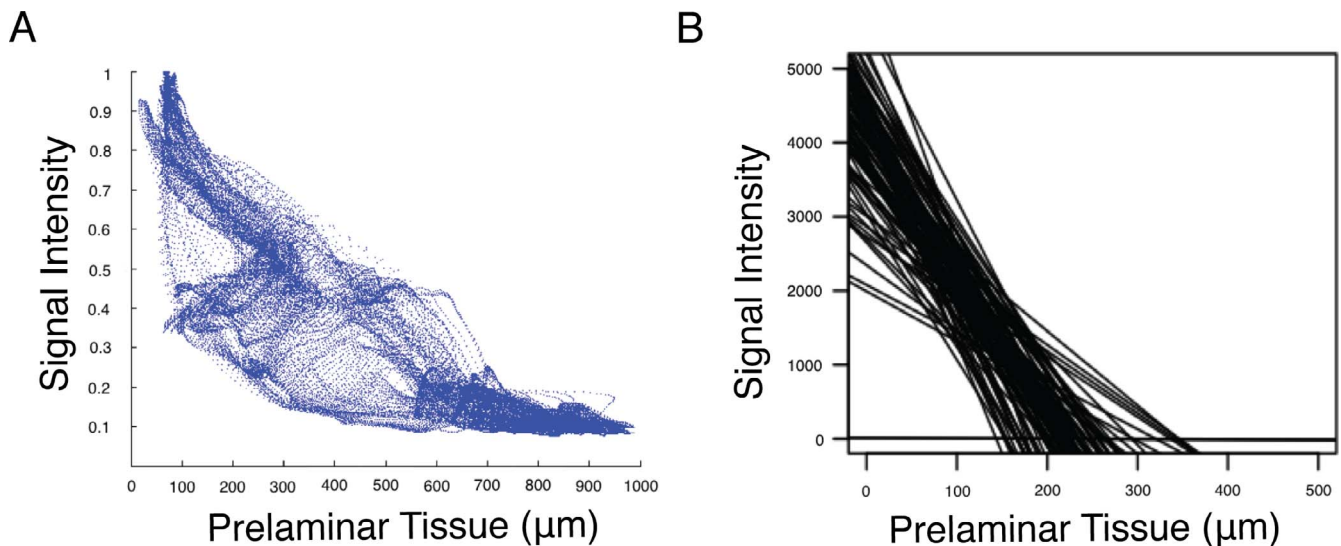
A

B

FIGURE 5. (**A**) Example of data from one eye representing the signal intensity on an individual superpixel basis compared to the prelaminar tissue thickness measured at the corresponding location. (**B**) Best fit lines from all 91 eyes, demonstrating the similarity in the trends of all eyes, with weaker signal in locations with thick prelaminar and stronger signal in locations with thinner prelaminar tissue.

disease, while eyes with more normal anatomy and thick prelaminar tissue were excluded due to poor LC visualization. This might skew some of the quantitative information reported about the LC. It should be noted that SS-OCT was used in this study, which has better tissue penetration than conventional SD-OCTs.[10] Therefore, our findings are expected to be further emphasized when SD-OCT is used for LC imaging.

By comparing the prelaminar thickness in regions of visible LC to the thickness in regions in which the LC was not visible in a given eye, we were able to isolate the effect of prelaminar tissue thickness, as potential confounders such as age, diagnosis, and media opacities would have the same effect on a given eye. Our finding that poor LC visibility is related to thick prelaminar tissue highlights a current limitation of OCT technology. Due to the safety limits of projected light, light scattering, and absorption, high quality images of the LC from eyes with thick prelaminar tissue are difficult to acquire at this time.

Much of the analysis presented in this study was done with manual delineation and subjective assessment. This is considered a limitation of this study, but at this time no other method has been developed to measure automatically the structures analyzed here. Efforts were made to limit bias and human error as much as possible. All measurements were made by an experienced observer who regularly analyzed OCT scans of the LC, and the observer was masked to all clinical information during scan assessment. The reproducibility of the observer was excellent. The analysis of the superpixel components of the scans correlated with regions where the LC was deemed to be analyzable or not analyzable, strengthening the validity of this manual designation. The ALC boundary was marked carefully in regions where the boundary was visible on the B-scan view, which largely corresponded to regions where the LC microstructure also was visible. Regions where the ALC was not considered visible that were included in the total prelaminar tissue thickness measurements were regions, such as seen in Figure 1C, colored in pink. For the purposes of this
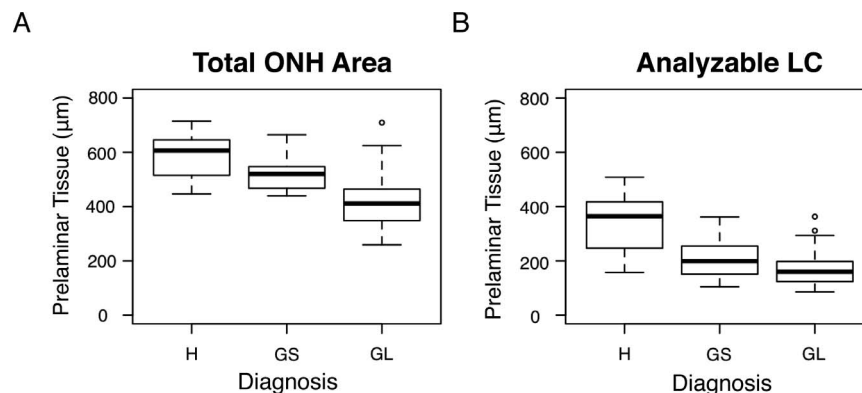
A

Total ONH Area

B

Analyzable LC

FIGURE 6. The average prelaminar tissue thickness of each diagnostic group for (**A**) the entire ONH region and (**B**) the regions that featured analyzable en face LC. A significant difference in total average prelaminar thickness (**A**) was seen between glaucaoma (GL) and healthy (H) eyes and glaucoma and glaucoma suspect (GS) eyes (both $P < 0.001$). The average prelaminar tissue thickness in regions where the LC was analyzable was significantly thinner in glaucoma eyes than glaucoma suspect and healthy eyes ($P = 0.008$ and $P < 0.001$, respectively), and glaucoma suspect eyes had significantly thinner prelaminar tissue than healthy eyes ($P < 0.001$).
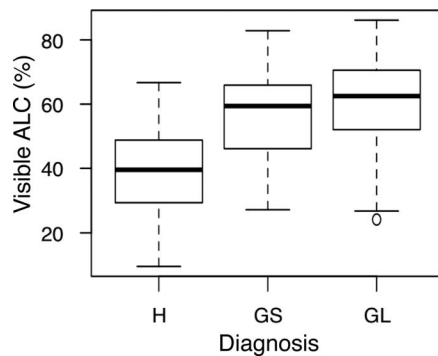
FIGURE 7. Average percentage of the visible ALC boundary seen in each scan over the region contained within Bruch's membrane opening for each diagnostic group. A significant difference was seen between GL and H eyes ($P = 0.005$).

study, we were interested in determining the amount of ALC boundary or LC microstructure that was visible in relation to the prelaminar tissue thickness of each eye. In the future, investigation into whether shadowed regions with thick prelaminar tissue also include blood vessel shadowing is warranted, as well as a calculation of what percentage of obscured ALC boundary is due to blood vessel shadowing.

Our study was designed to concentrate on the effect of prelaminar tissue on LC visibility. Because most literature focuses on the visible LC within the BMO, our analysis also was limited to the region within the BMO. Therefore, caution should be exercised when relating our results to the entire prelaminar tissue area since the lateral aspect, outside the BMO, was not analyzed. Furthermore, the region outside the BMO also is prone to high signal variability, which makes peripheral marking of the ALC unreliable or impossible in some scans; thus, reducing the reliability of the analysis.

Lamina cribrosa visibility is predominantly problematic in studies that quantify its structure across their cohort because LC visualization differs for each eye inherently based on the amount of prelaminar tissue that the eye has. Furthermore, depending on the location of regions of thick prelaminar tissue, different regions of the LC are analyzed in different eyes. Because LC microstructure varies spatially,[26,27] differences in the regions of analyzable LC between eyes can impact the outcome of analyses. Therefore, it may be better to use LC analysis for the assessment of longitudinal progression changes in the same eye rather than for cross-sectional LC analysis between eyes. In this situation, better LC visualization could be used independently as an indication of tissue loss with disease.

In conclusion, thicker prelaminar tissue was associated with significantly lower LC visibility. As significant differences in prelaminar tissue thickness exist between diagnostic categories, there could be an inherent bias in any LC analysis for selecting subjects with thinner prelaminar tissue. It is important to take these considerations into account in future studies of the LC, as well as to develop methods to mitigate this potential selection bias in cross-sectional studies of the LC.

Acknowledgments

Disclosure: **K.A. Lucy**, None; **B. Wang**, None; **J.S. Schuman**, Zeiss (R), P; **R.A. Bilonick**, None; **Y. Ling**, None; **L. Kagemann**, None; **I.A. Sigal**, None; **I. Grulkowski**, None; **J.J. Liu**, Topcon (E); **J.G. Fujimoto**, Zeiss (R), Optovue (I), P; **H. Ishikawa**, None; **G. Wollstein**, None

References

1. Burgoyne CF. A biomechanical paradigm for axonal insult within the optic nerve head in aging and glaucoma. *Exp Eye Res*. 2011;93:120–132.

2. Quigley HA, Addicks EM, Green WR, Maumenee AE. Optic nerve damage in human glaucoma. II. The site of injury and susceptibility to damage. *Arch Ophthalmol*. 1981;99:635–649.

3. Quigley HA, McKinnon SJ, Zack DJ, et al. Retrograde axonal transport of BDNF in retinal ganglion cells is blocked by acute IOP elevation in rats. *Invest Ophthalmol Vis Sci*. 2000;41:3460–3466.

4. Burgoyne CF, Crawford Downs J, Bellezza AJ, Francis Suh J-K, Hart RT. The optic nerve head as a biomechanical structure: a new paradigm for understanding the role of IOP-related stress and strain in the pathophysiology of glaucomatous optic nerve head damage. *Prog Retin Eye Res*. 2005;24:39–73.

5. Sigal IA, Ethier CR. Biomechanics of the optic nerve head. *Exp Eye Res*. 2009;88:799–807.

6. Huang D, Swanson EA, Lin CP, et al. Optical coherence tomography. *Science*. 1991;254:1178–1181.

7. Schuman JS, Pedut-Kloizman T, Pakter H, et al. Optical coherence tomography and histologic measurements of nerve fiber layer thickness in normal and glaucomatous monkey eyes. *Invest Ophthalmol Vis Sci*. 2007;48:3645–3654.

8. Spaide RF, Koizumi H, Pozonni MC. Enhanced depth imaging spectral-domain optical coherence tomography. *Am J Ophthalmol*. 2008;146:496–500.

9. Srinivasan VJ, Adler DC, Chen Y, et al. Ultrahigh-speed optical coherence tomography for three-dimensional and en face imaging of the retina and optic nerve head. *Invest Ophthalmol Vis Sci*. 2008;49:5103–5110.

10. Choma M, Sarunic M, Yang C, Izatt J. Sensitivity advantage of swept source and Fourier domain optical coherence tomography. *Opt Express*. 2003;11:2183–2189.

11. Lim H, Chen TC, de Boer JF, et al. High-speed imaging of human retina in vivo with swept-source optical coherence tomography. *Opt Express*. 2006;14:12902–12908.

12. Yasuno Y, Hong Y, Makita S, et al. In vivo high-contrast imaging of deep posterior eye by 1-um swept source optical coherence tomography and scattering optical coherence angiography. *Opt Express*. 2007;15:6121–6139.

13. Lee EJ, Kim T-W, Weinreb RN, Park KH, Kim SH, Kim DM. Visualization of the lamina cribrosa using enhanced depth imaging spectral-domain optical coherence tomography. *Am J Ophthalmol*. 2011;152:87–95.

14. Nadler Z, Wang B, Wollstein G, et al. Automated lamina cribrosa microstructural segmentation in optical coherence tomography scans of healthy and glaucomatous eyes. *Biomed Opt Express*. 2013;4:2596–2608.

15. Sigal IA, Wang B, Strouthidis NG, Akagi T, Girard MJA. Recent advances in OCT imaging of the lamina cribrosa. *Br J Ophthalmol*. 2014;98:34–39.

16. Potsaid B, Baumann B, Huang D, et al. Ultrahigh speed 1050nm swept source/Fourier domain OCT retinal and anterior segment imaging at 100,000 to 400,000 axial scans per second. *Opt Express*. 2010;18:20029–20048.

17. Kraus MF, Potsaid B, Mayer MA, et al. Motion correction in optical coherence tomography volumes on a per A-scan basis using orthogonal scan patterns. *Biomed Opt Express*. 2012;3:1182–1189.

18. Schindelin J, Arganda-Carreras I, Frise E, et al. Fiji: an open-source platform for biological-image analysis. *Nat Methods*. 2012;9:676–682.

19. Wang B, Nevins JE, Nadler Z, et al. In vivo lamina cribrosa micro-architecture in healthy and glaucomatous eyes as assessed by optical coherence tomography. *Invest Ophthalmol Vis Sci*. 2013;54:8270–8274.

20. Buchser NM, Wollstein G, Ishikawa H, et al. Comparison of retinal nerve fiber layer thickness measurement bias and imprecision across three spectral-domain optical coherence tomography devices. *Invest Ophthalmol Vis Sci*. 2012;53: 3742–3747

21. MATLAB. Natick, Massachusetts: The MathWorks Inc.; 2015. Available at: https://www.mathworks.com/.

22. R Core Team. R: A language and environment for statistical computing. Vienna, Austria: R Foundation for Statistical Computing; 2015. Available at: https://www.R-project.org/.

23. Wu Z, Xu G, Weinreb RN, Yu M, Leung CKS. Optic nerve head deformation in glaucoma: a prospective analysis of optic nerve head surface and lamina cribrosa surface displacement. *Ophthalmology*. 2015;122:1317–1329.

24. Agoumi Y, Sharpe GP, Hutchison DM, Nicolela MT, Artes PH, Chauhan BC. Laminar and prelaminar tissue displacement during intraocular pressure elevation in glaucoma patients and healthy controls. *Ophthalmology*. 2011;118:52–59.

25. Barrancos C, Rebolleda G, Oblanca N, Cabarga C, Muñoz-Negrete FJ. Changes in lamina cribrosa and prelaminar tissue after deep sclerectomy. *Eye Lond Engl*. 2014;28:58–65.

26. Wang B, Nevins JE, Nadler Z, et al. In vivo lamina cribrosa micro-architecture in healthy and glaucomatous eyes as assessed by optical coherence tomography. *Invest Ophthalmol Vis Sci*. 2013;54:8270–8274.

27. Nadler Z, Wang B, Schuman JS, et al. In vivo three-dimensional characterization of the healthy human lamina cribrosa with adaptive optics spectral-domain optical coherence tomography. *Invest Ophthalmol Vis Sci*. 2014;55:6459–6466.